Supplementary Information

The ‘Supplementary Information’ file includes 5 sections:

1. Coulomb Failure Stress
2. Three-dimensional Finite Element modelling
3. Modelling of Coulomb Failure Stress due to intraplate earthquakes
4. Additional Results
5. Further remarks

It also includes 3 equations and additional references.

Supplementary Figures

Supplementary Figures contain 6 figures and their captions.

Supplementary Tables

Supplementary Tables contains one table and its caption.

Climate change-induced earthquakes in northern Central Europe: Supplementary Information

Christian Brandes[1], Holger Steffen[2], Rebekka Steffen[3] and Patrick Wu[4]

[1]Institut für Geologie, Leibniz Universität Hannover, Callinstraße, 30167 Hannover, Germany

[2]Lantmäteriet, Informationsförsörjning Geodesi Referenssystem, Lantmäterivägen 2c, 80102 Gävle, Sweden

[3]Department of Geosciences, Uppsala University, Villavägen 16, 75236 Uppsala, Sweden

[4]Department of Earth Sciences, The University of Hong Kong, Pokfulam Road, Hong Kong

1. Coulomb Failure Stress

Our description below of the Coulomb Failure Stress (CFS, Supplementary Fig. S1) summarizes the detailed description in Steffen et al. (2014a).

Failure occurs at the point where the Mohr circle touches the failure envelope $|\tau| = f(\sigma_n)$. For most practical applications, the failure envelope can be approximated linearly by an equation which relates a certain critical value τ_c to the shear stress along a fault plane:

$$|\tau_c| = S + \mu\sigma_n, \tag{1.1}$$

where μ is the internal coefficient of friction, σ_n is the normal stress applied to the fault plane and *S* is the cohesion strength. Since the line of failure is tangent to the Mohr circle, the orientation of the fault plane is given by: $tan(2\theta) = 1/\mu$ (e.g. Ranalli 1995, p.100).

The total stress field that is represented by the Mohr circle consists of the time-dependent rebound stresses (induced by glacial cycles) superimposed on the time-independent ambient stresses which include tectonic stress and the vertical normal stress due to overburden and fluid pressure. Since the total stress changes in time, faults that are initially close to failure will not remain so.

To further evaluate δCFS, we have to consider the stress evolution inside and outside the ice margin, respectively, as well as the three main types of faults, or fault regimes: normal-faulting, strike-slip or thrust-faulting. They are distinguished by whether the vertical stress is the maximum, intermediate or minimum principal stress, respectively. As shown below, δCFS at a location near the glaciated area, i.e. in an area up to 500 km around the former ice sheet, follows a similar behaviour like a location inside the former ice sheet. Therefore, we only discuss this behaviour.

During glacial loading (Supplementary Fig. S2a), the weight of the ice sheet increases the mean stress, i.e. the stress in all three principal stress components σ_1, σ_2 and σ_3, but the change in stress difference is generally small, so that the centre of the Mohr circle moves to the right but the radius of the Mohr circle is almost unchanged. Therefore, the Mohr circle moves away from the line of failure (Johnston 1987, 1989) and pre-existing faults become more stable. After the end of deglaciation, the horizontal principal stress remains large (because of the induced flexural stress in addition to ambient stresses) even when the weight of the ice sheet disappeared. For a thrust regime (Supplementary Fig. S2b) where the vertical stress is the minimum principal stress σ_3 and the maximum horizontal stress is the maximum principal stress σ_1, the stress difference of both, i.e. the diameter of the Mohr circle, increases while the vertical stress returns to its initial value. Thus, the Mohr circle comes closer to the line of failure or actually reaches it after deglaciation.

For strike-slip regime where the vertical stress is the intermediate principal stress (Supplementary Fig. S2c), flexure causes both σ_1 and σ_3, in this case the maximum and minimum horizontal stresses, respectively, to increase after deglaciation – as a result there is not much change towards failure. For normal faulting where the vertical stress is the maximum principal stress σ_1 and the minimum horizontal stress is the minimum principal stress σ_3 (Supplementary Fig. S2d), the fault is more stable than the initial state after deglaciation and thus failure is not expected.

The CFS represents the vertical distance between the Mohr circle of a stress field and the failure criterion (Supplementary Fig. S1). If the value of the CFS decreases (i.e. the change in Coulomb Failure Stress, δCFS, decreases) during stress evolution, it means the fault has become more stable and the potential for fault activation decreases. On the other hand, a positive change, or an increasing CFS (δCFS > 0, i.e. the distance between failure criterion and Mohr circle becomes smaller) means that the fault becomes less stable and the potential for fault activation increases. According to Harris (1998), the CFS is related to the principal compressive stresses by:

$$\mathrm{CFS} = \tau + \mu \sigma_n - S \,. \qquad (1.2)$$

Due to difficulties in estimating the value of cohesion *S*, Wu & Hasegawa (1996) proposed to study instead a change of the failure criterion, which can be applied to CFS at time *t* relative to that at initial time t_o:

$$\delta\mathrm{CFS}(t) = \mathrm{CFS}(t) - \mathrm{CFS}(t_o) = \tau(t) - \tau(t_0) + \mu(\sigma_n(t) - \sigma_n(t_0)) \qquad (1.3)$$

This is possible due to the fact that the stress evolves continuously during a glacial cycle, and so does the value of CFS with time. δCFS is simply the difference between CFS at the time under consideration and the initial value of CFS before the onset of glacial cycles, and it characterizes the effect of the glacial cycle on the stability of faults.

We assume the following conditions for computation of δCFS in this study:

- Glacial unloading are not large enough to fracture intact rocks - only pre-existing faults can be reactivated. This implies that are the faults are initially close to failure with value of S close to zero.
- In the GIA model, the pre-existing faults are considered to be "virtual faults", i.e. their presence do not affect the state of stress. However, recent models with more realistic non-virtual faults do support our finding here (Steffen et al., 2014b).
- Changes in fluid pressure and lithostatic pressure can affect fault activation. So to keep the problem simple, they are assumed to be time independent. (e.g. Wu & Hasegawa,1996).

2. Three-dimensional Finite Element modelling

The Boussinesq problem is solved with the finite element (FE) software ABAQUS for a layered, laterally heterogeneous, viscoelastic half-space with isotropic, compressible material properties. The ABAQUS FE model has been modified to include pre-stress advection (according to Wu 1992a,b, 2004) in order to allow the deformed free surface to return to its initial equilibrium via viscous flow. The basic model U1L1_V1, its material parameters based on the Preliminary Reference Model (PREM, Dziewonski & Anderson 1981) and dimensions are described in Steffen et al. (2006). It is a model with a 70 km lithosphere and no lateral variation in viscosity of the upper or lower mantle (which are subdivided at 670 km depth): Upper-mantle viscosity is set to 4×10^{20} Pa s and lower-mantle viscosity to 2×10^{22} Pa s. The lateral viscosity structure of the two models U3L3_V1 and U3L3_V3 can be found in

Steffen et al. (2006) as well. These structures are derived from the shear-wave velocity perturbations in the S20A tomographical model (Ekström and Dziewonski, 1998) and for U3L3_V1 from the vertical background viscosity from model U1L1_V1, and for U3L3_V3 from a viscosity profile based on mineral physics and heat conduction results. The ice-load history is based on model FBKS8 by Lambeck et al. (1998). Its implementation is also described in Steffen et al. (2006).

These three models were used for calculation of δCFS as they fit the GPS-derived velocity field and relative sea-level data for Fennoscandia reasonable well (Steffen et al. 2006) and also cover reasonable model configurations for GIA in Fennoscandia. The δCFS calculation is based on the stress and displacement results of the FE model computation of Steffen et al. (2014a) with all faults initially close to failure.

3. Modelling of Coulomb Failure Stress due to intraplate earthquakes

The software Coulomb 3.3 (Stein 2003) computes Coulomb stress changes due to earthquakes. The stress changes are calculated using the fault-slip value, fault geometry and Young's modulus. The first two parameters are used in the estimation of the displacement behavior using the method by Okada (1992), assuming an elastic halfspace. The stress changes are then calculated from the Young's modulus and strain field, which is obtained from the displacement behavior. Although the original intended purpose is to obtain the static displacement and strain parameters, we mainly use it to analyze the promotion or inhibition of failure on nearby faults due to an earthquake – i.e. how the CFS changes along the faults.

Former studies (King et al. 1994, Árnadóttir et al. 2003, Lin & Stein 2004) showed that the CFS change on nearby faults due to an earthquake event is mostly below 1 MPa but it also depends on the distance of the activated fault to the nearby fault. Studies of Coulomb stress changes in Iceland have shown that parallel strike-slip faults may affect each other (Árnadóttir et al., 2003). An intermediate earthquake with a surface magnitude of 6.6 induced a positive CFS of +0.2 MPa, and thus increased instability at a parallel fault 20 km away, triggering an earthquake there shortly afterwards (Árnadóttir et al., 2003).

In order to study the effect of an earthquake on the change in CFS at all depth along nearby faults in Central Europe, we consider the fault distribution as shown in Supplementary Fig. S3 and their parameters in Supplementary Table S1. All faults except the Gardelegen fault are not blind and are supposed to strike out at the surface. The crustal parameters are the same as the elastic parameters used in the ABAQUS models, and a coefficient of friction of 0.6 (Byerlee, 1978) is used. Different amounts of slips are assumed along the faults, and their magnitudes are based on studied intraplate thrust earthquakes around the world (Wells & Coppersmith, 1994). Our results show that earthquakes investigated have negligible effect on nearby faults. Consider, for example, the Haldensleben and Gardelegen Faults which are closest to each other, with a distance of only 15 km. An earthquake at the Haldensleben Fault induces Coulomb stress changes of -0.08 MPa when a maximum slip of 1.5 m is assumed. This change in Coulomb stress would move the Gardelegen fault towards stability, but this change is small when compared to the overall CFS on the original fault. For larger separation between the faults, the Coulomb stress change on other faults is even smaller.

4. Additional results

Supplementary Fig. S4 shows the spatio-temporal evolution of δCFS in northern and central Europe at 12 selected times for the three earth models used under thrust-fault mechanism. At LGM (21.8 ka) whole northern Europe has negative values and is thus considered stable. Largest values arise in the glaciated area, which confirms the discussion in Supplementary Sect. 1 and Supplementary Fig. S2. With retreating ice, the stable (negative) area becomes smaller and positive values appear at the ice margin and outside of the formerly glaciated area up to 500 km distance. The pattern and timing of transition from negative to positive values depends on the background viscosity model used. There are some similarities among the model predictions especially at older times, however larger differences are found in the marginal areas during postglacial times. For example, the forebulge area in the 3D models (U3L3_V1 and U3L3_V3) in the northwest of Norway results in negative values from around 8 ka till the present. However, in the area of interest in this study, i.e. central Europe, Denmark and the southern tip of Sweden, there are only small differences in the behaviour between the two 3D models, which mainly differs in the time when δCFS=0. Another interesting point is the strong increase of about 6 MPa in northern Sweden from 11.3 ka to 10 ka (all models show this behaviour), which moves the area from stable conditions to unstable. This would explain the expected strong earthquakes around that time which led to the formation of the postglacial faults in the area (see e.g. Lagerbäck & Sundh, 2008). Hence, our model is able to describe the driving mechanism for these well-known postglacial faults as well as the now identified postglacial faults in northern Central Europe.

Supplementary Fig. S5 shows the δCFS for a model (U1L1_V1) in a normal-fault regime. Within the (formerly) glaciated area, δCFS is predicted to be mostly stable from LGM to today. Outside the former ice margin, regions of instability are predicted. However, the region of stability expands outwards in time. The prediction within the ice margin is in direct contradiction to the existence of the postglacial thrust faults in northern Scandinavia, which indicate that earthquakes actually occurred near the end of deglaciation. Furthermore, thrusting events during the last 1200 years in Central Europe also indicate that we can exclude normal-fault mechanism in our analysis.

In addition to the results in Fig. 3 of the main text, Supplementary Fig. 6 presents the time evolution of δCFS for other epicentres in Fig. 2. They additionally confirm our hypothesis introduced in the main part. Furthermore, independent of the assumed fault slip of a first event, they indicate that any earthquake activity today may be most likely related to GIA.

5. Further remarks

All intensities in this study are based on the MSK-64 Scale and for the younger events on the EMS-98 Scale (Leydecker, 2011).

References

Árnadóttir, T., Jónsson, S., Pedersen, R. & Gudmundsson, G.B. Coulomb stress changes in the South Iceland Seismic Zone due to two large earthquakes in June 2000. *Geophys. Res. Lett.* **30** (5), 1205 (2003).

Byerlee, J.D. Friction of rock. *Pure Appl. Geophys.* **116**, 615-626 (1978).

Dziewonski, A. M. & Anderson D. L. Preliminary reference Earth model. *Phys. Earth Planet. Inter.* **25**, 297–356 (1981).

Ekström, G., & Dziewonski, A.M. The unique anisotropy of the Pacific upper mantle. *Nature* **394**, 168–172 (1998).

Harris, R.A. Introduction to Special Section: Stress Triggers, Stress Shadows, and Implications for Seismic Hazard. *J. Geophys. Res.* **103**, 24347–24358 (1998).

Johnston, A.C. Suppression of earthquakes by large continental ice sheets. *Nature* **330**, 467-469 (1987).

Johnston, A.C. The seismicity of “stable” continental interiors. In: Gregersen, S. & Basham, P.W. (eds.) *Earthquakes at North Atlantic Passive Margins: Neotectonics* *and Post-Glacial Rebound*, NATO ASI Series C, Mathematical and Physical Sciences, 563-579 (1989).

King, G.C.P., Stein, R.S. & Lin, J. Static stress changes and the triggering of earthquakes, *Bull. Seismol. Soc. Amer.* **84**(3), 935-953 (1994).

Lagerbäck, R. & Sundh, M. Early Holocene faulting and paleoseismicity in Northern Sweden. Sveriges geologiska undersökning – Research paper **836** (2008).

Lambeck, K., Smither, C. & Johnston, P. Sea-level change, glacial rebound and mantle viscosity for northern Europe. *Geophys. J. Int.* **134**, 102-144 (1998).

Leydecker, G. Erdbebenkatalog für die Bundesrepublik Deutschland mit Randgebieten für die Jahre 800-2008. *Geologisches Jahrbuch Reihe E*, 198 pp. (2011)

Lin, J. & Stein, R.S. Stress triggering in thrust and subduction earthquakes, and stress interaction between the southern San Andreas and nearby thrust and strike-slip faults. *J. Geophys. Res.* **109**, B02303 (2004).

Okada, Y. Internal deformation due to shear and tensile faults in a half-space: Bulletin of the Seismological Society of America, v. 82, no. 2, p. 1018-1040 (1992).

Ranalli, G. *Rheology of the Earth*. Chapman & Hall, London (1995).

Stein, R.S. Earthquake conversations, *Scientific American* **288** (1), 72-79 (2003).

Steffen, H., Kaufmann G. & Wu, P. Three-dimensional finite-element modelling of the glacial isostatic adjustment in Fennoscandia. *Earth Planet. Sci.Lett.* **250**, 358–375 (2006).

Steffen, R., Wu, P., Steffen, H. & Eaton, D.W. On the implementation of faults in finite-element glacial isostatic adjustment models. *Comput. Geosci.* **62**, 50–59 (2014a).

Steffen, R., Wu, P., Steffen, H. & Eaton., D. W. The effect of earth rheology and ice-sheet size on fault-slip and magnitude of postglacial earthquakes. *Earth Planet. Sci. Lett.* **388**, 71–80 (2014b).

Wells, D.L. & Coppersmith, K.J. New Empirical Relationships among Magnitude, Rupture Length, Rupture Width, Rupture Area, and Surface Displacement. *Bull. Seismol. Soc. Am.*, **84** (4), 974-1002 (1994).

Wu, P. Deformation of an incompressible viscoelastic flat Earth with power-law creep: a finite element approach. *Geophys. J. Int.* **108**, 35-51 (1992a).

Wu, P. Viscoelastic versus viscous deformation and the advection of pre-stress. *Geophys. J. Int.* **108**, 136-142 (1992b).

Wu, P. Using commercial Finite element packages for the study of earth deformations, sea levels and the state of stress. *Geophys. J. Int.* **158**(2), 401-408 (2004).

Wu, P. State-of-the-Science Review of the Stress Field during a Glacial Cycle and Glacial Induced Faulting. Technical Report TR-2010-XX prepared by Department of Geoscience, University of Calgary for the Nuclear Waste Management Organisation, (2010). (Available at www.nwmo.ca)

Wu, P. & Hasegawa. H.S. Induced stresses and fault potential in Eastern Canada due to a disc load: a preliminary analysis. *Geophys. J. Int.* **125**, 415-430 (1996).

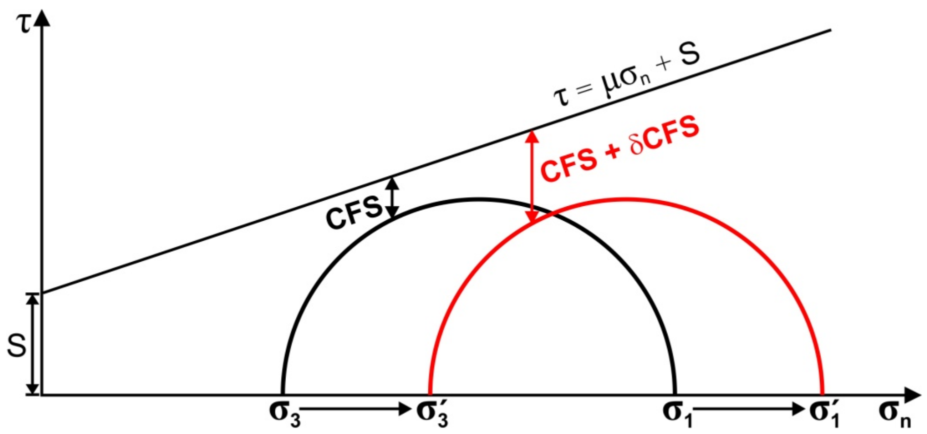

Supplementary Figure S1: Mohr circle for the state of stress showing the Coulomb Failure Stress (CFS) and the relationship between normal stress σ_n and shear stress τ. σ_1 and σ_3 are the maximum and minimum stresses, respectively. The sloping line represents Coulomb's failure criterion with S as the cohesion strength and μ as the internal coefficient of friction. Brittle failure occurs when Mohr circle touches the failure envelope. The Coulomb Failure Stress (CFS) is the distance from the circle to the line of failure and can change over time (red circle) if the differential stress varies. The Mohr Circle for different stress regimes after deglaciation can be found in Supplementary Fig. S2.

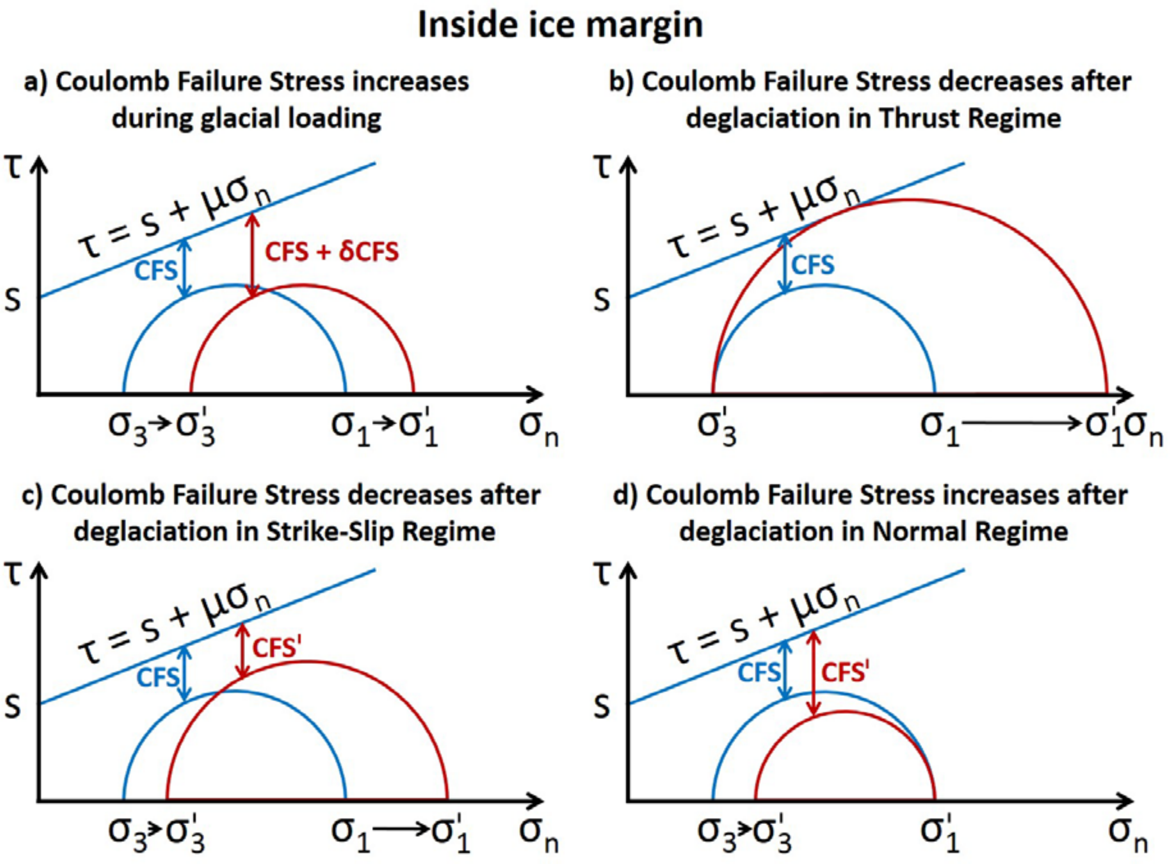

Supplementary Figure S2: Coulomb Failure Stress and its change during a glacial cycle for a site inside the ice margin of a large ice sheet. σ_1 and σ_3 are the maximum and minimum principal stresses of the ambient stress field before a glacial cycle, but the primed quantities are those for the total (ambient and glacial) stress field during glacial loading (a), and after deglaciation in (b) thrust, (c) strike-slip and (d) normal fault regime.

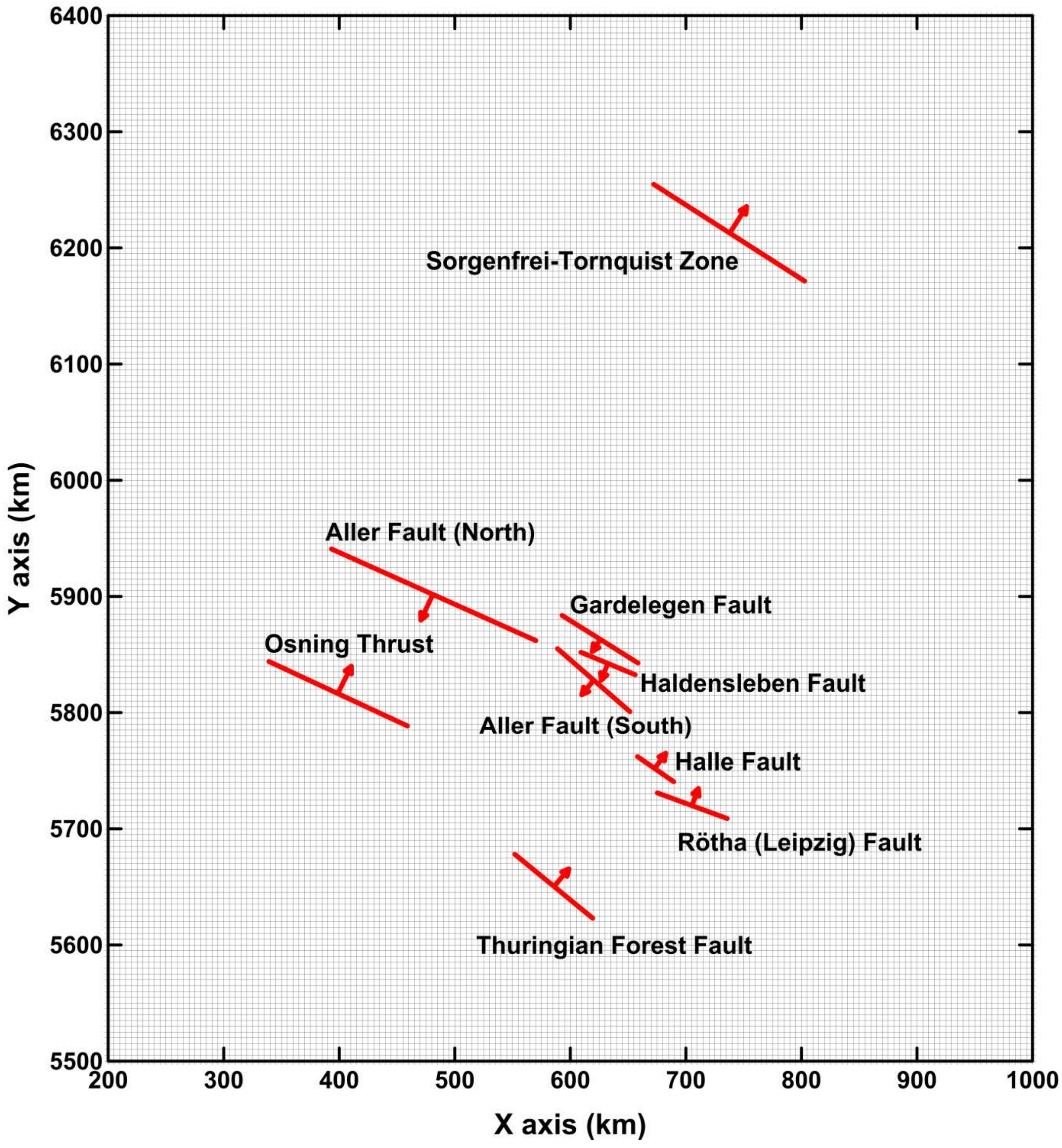

Supplementary Figure S3: Two-dimensional view of model used in Coulomb 3.3 (Stein, 2003) for the calculation of CFS due to an earthquake. The faults are named and the dip direction is indicated with arrows. The grid used in Coulomb 3.3 is underlain. The same coordinates as in Fig. 1 are used.

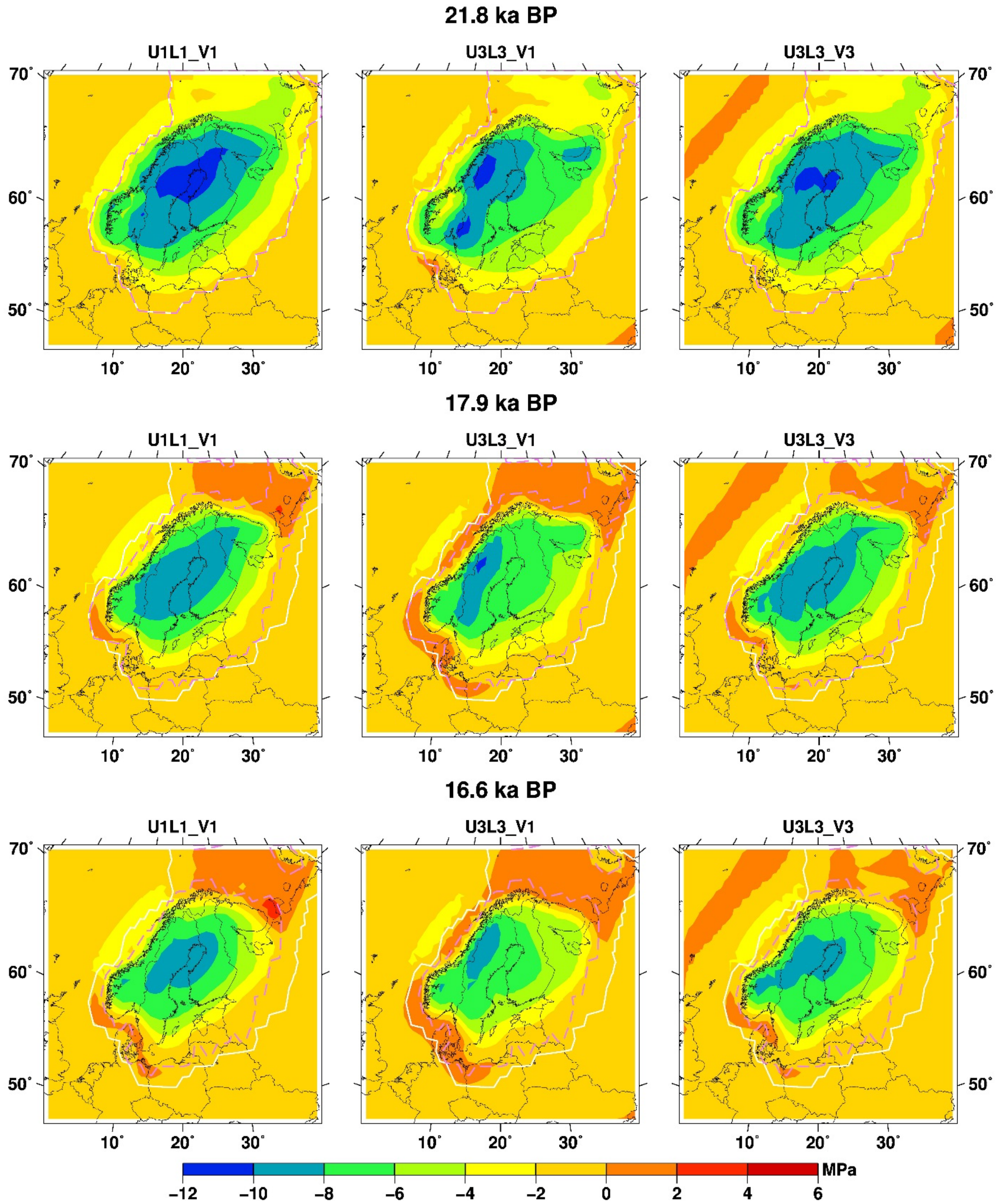

Supplementary Figure S4: δCFS in Fennoscandia at 12 selected times for models U1L1_V1, U3L3_V1 and U3L3_V3 with thrust-faulting background stress field in a seismogenic depth of 10 km. The solid white line sketches the maximum extent of the FBKS8 ice model, and the dashed violet line its extent at the time indicated (Lambeck et al. 1998).

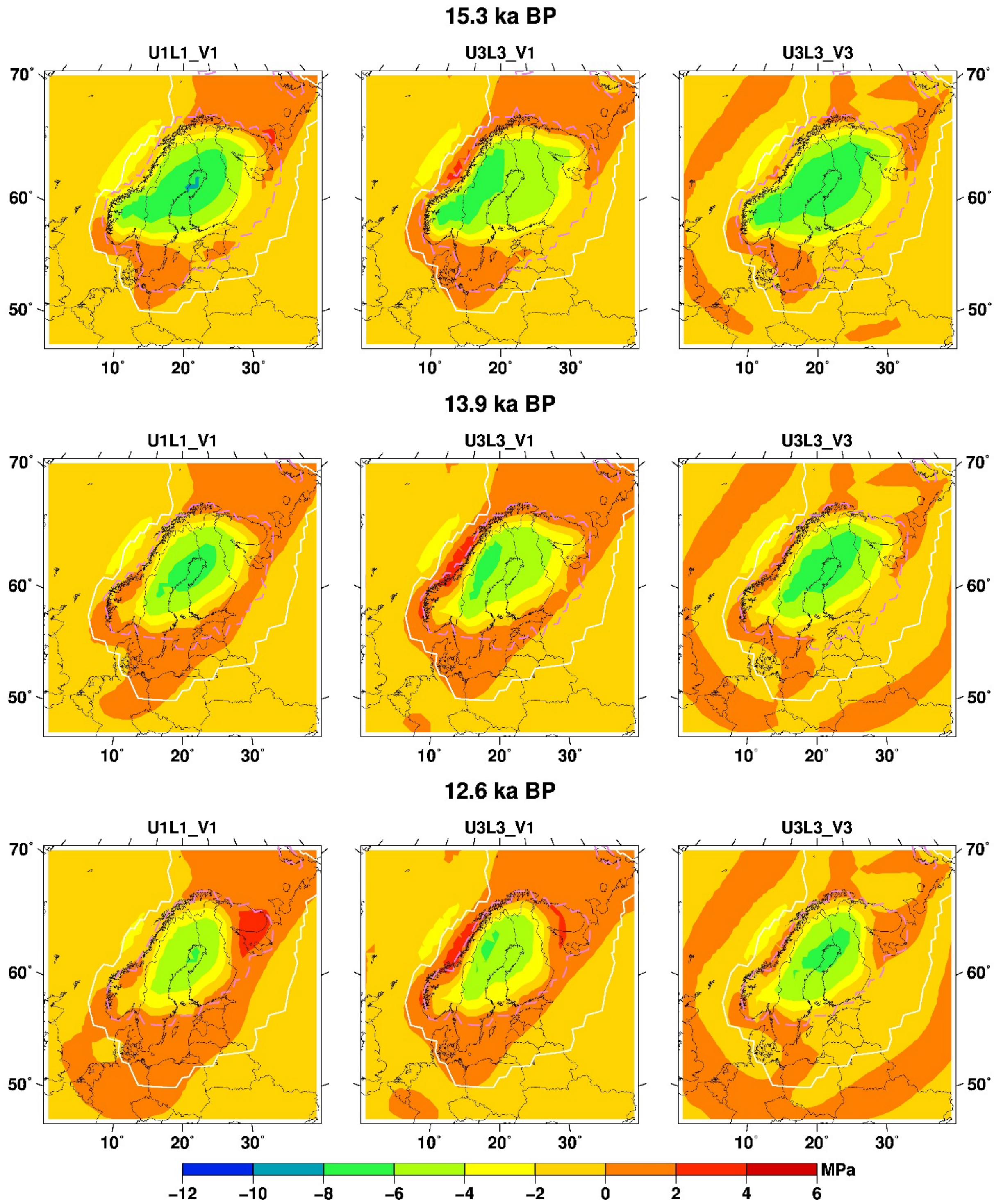

Supplementary Figure S4 continued.

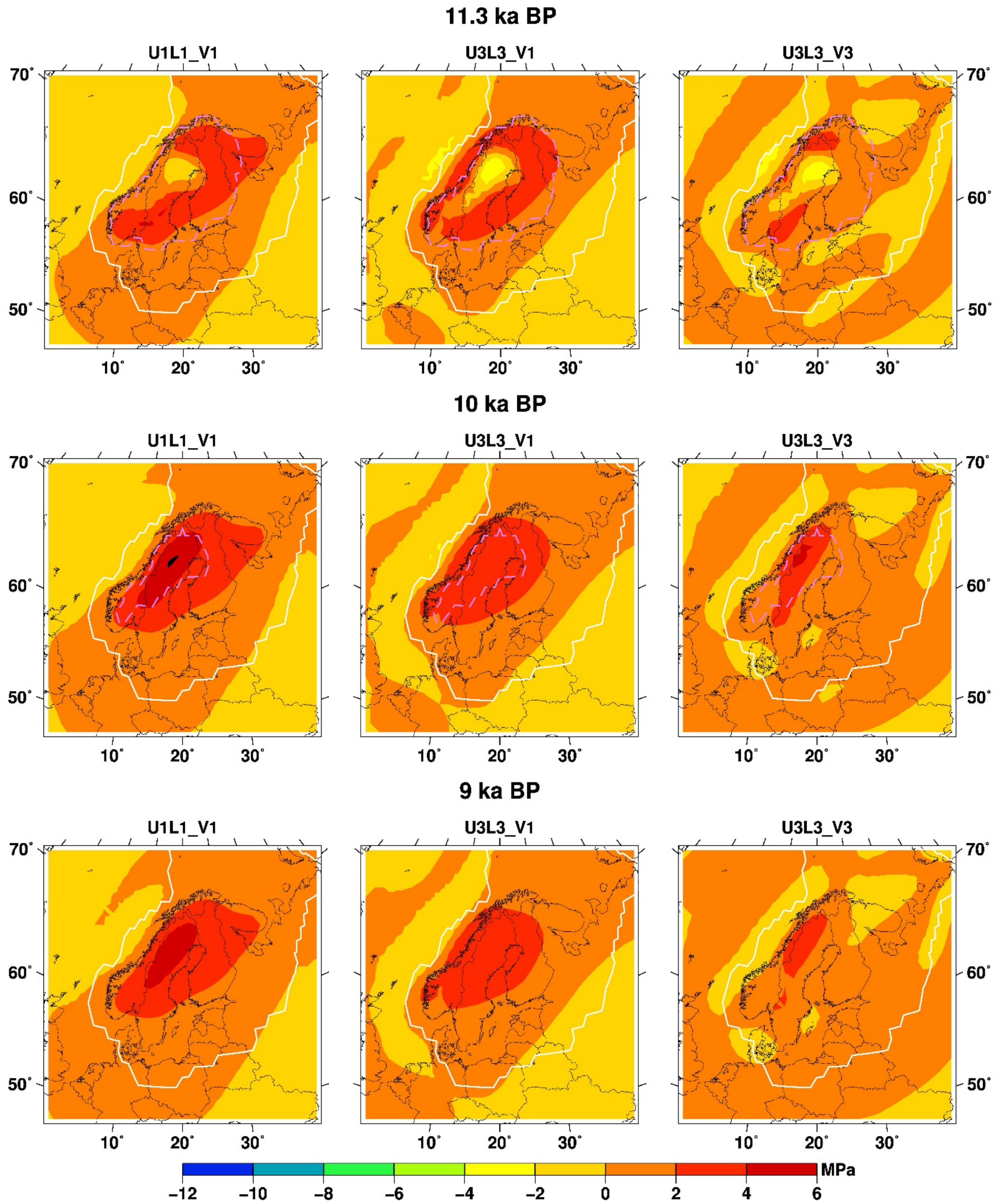

Supplementary Figure S4 continued.

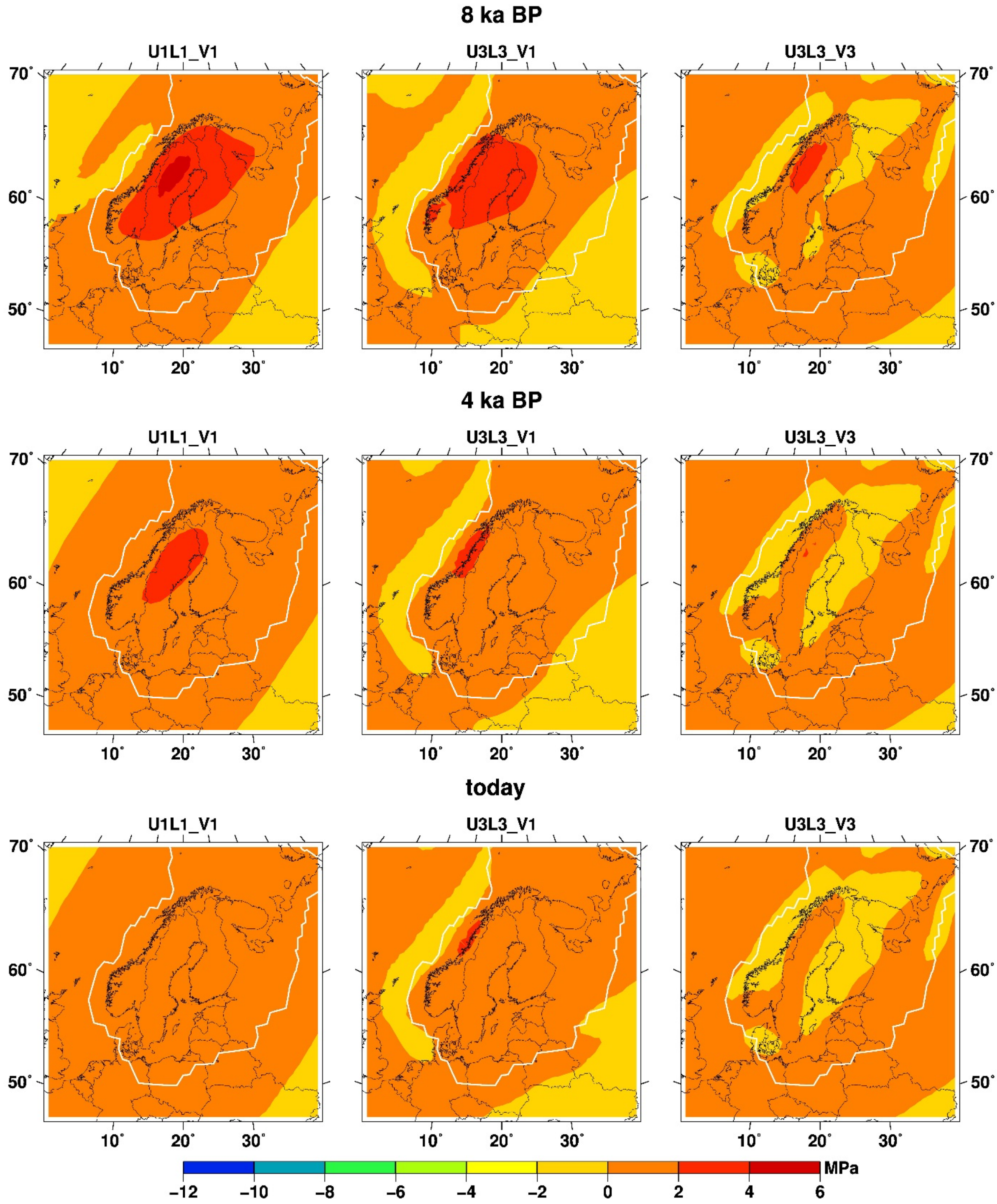

Supplementary Figure S4 continued.

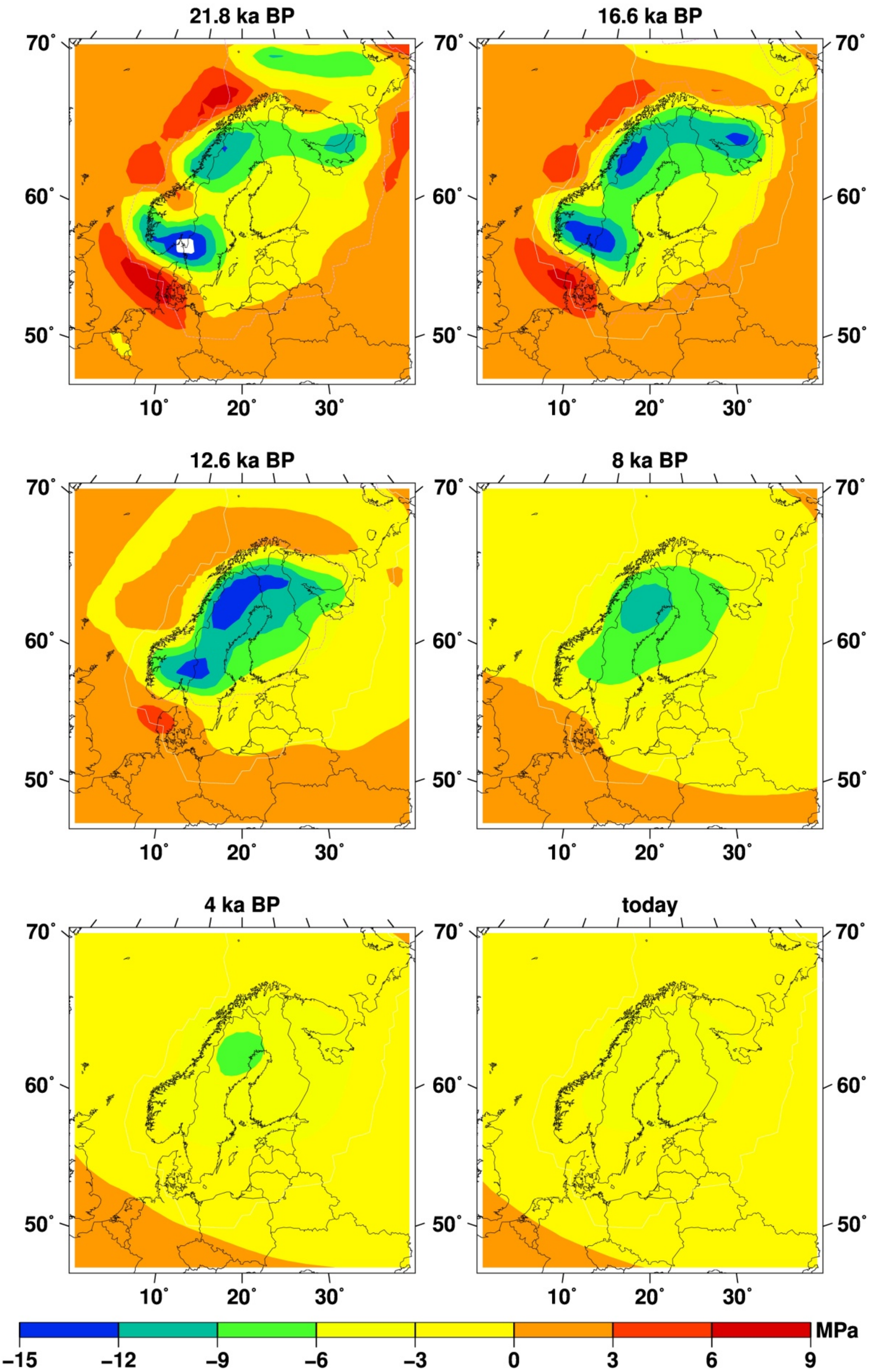

Supplementary Figure S5: Same as Supplementary Fig. S4, but for model U1L1_V1, normal fault regime and 6 times only.

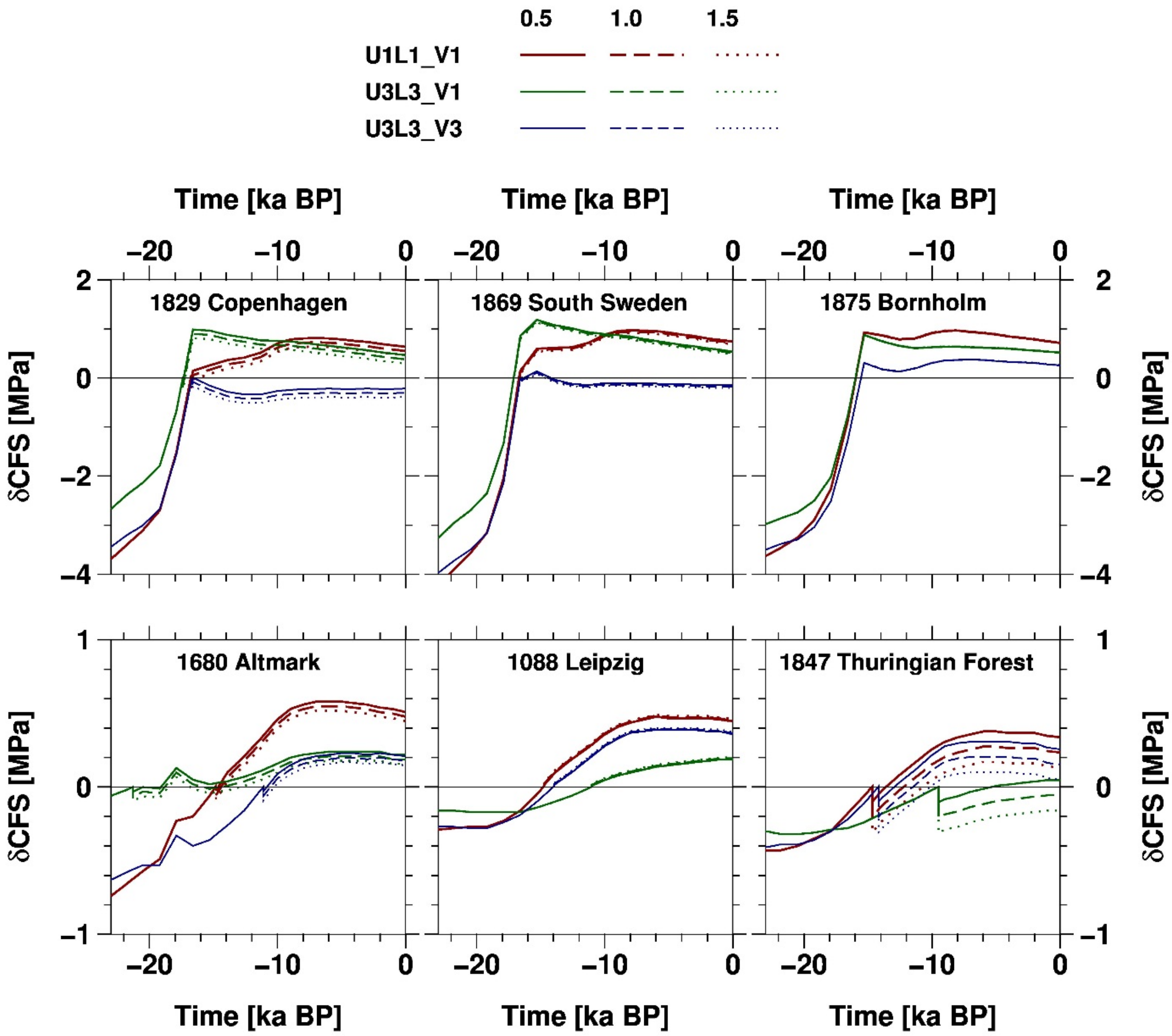

Supplementary Figure S6. Change in Coulomb Failure Stress for a thrust-fault regime for major reverse faults in northern Central Europe, Denmark and southern Sweden induced by the Weichselian glaciation in the last 23 ka and the effect of the first fault slip. Faults that showed historic seismicity in Germany (Altmark, Leipzig, and Thuringian Forest) mainly reach δCFS=0 between 15 ka BP and 10 ka BP. In contrast, at the Sorgenfrei-Tornquist Zone in Denmark and Sweden δCFS=0 was already reached between 17 ka BP and 16 ka BP. Numbers indicate typical intraplate fault slips in m used in Coulomb 3.3 (Stein, 2003) to calculate δCFS from earthquakes.

Supplementary Table S1. List of fault parameters used as input for Coulomb 3.3 (Stein, 2003).

Fault name	Length [km]	Blind	Depth [km]	Strike [°]	Dip [°]	Rake [°]	Fault slip [m]		
Sorgenfrei-Tornquist Zone	160	No	20	300	30	90	0.5	1.0	1.5
Osning Thrust	130	No	25	295	30	90	1.0	1.2	1.5
Thuringian Forest Fault	90	No	10	310	50	90	0.5	1.0	1.5
Aller Fault (North)	190	No	16	115	30	90	0.5	1.0	1.5
Aller Fault (South)	85	No	5	130	55	90	0.5	1.0	1.5
Gardelegen Fault	80	Yes	0.2 – 20	120	35	90	0.5	1.0	1.5
Halle Fault	40	No	10	305	50	90	0.5	1.0	1.5
Rötha Fault (Leipzig)	65	No	10	290	50	90	0.5	1.0	1.5
Haldensleben Fault	50	No	20	113	35	90	0.5	1.0	1.5